

Gapped triplet p -wave superconductivity in strong spin-orbit-coupled semiconductor quantum wells in proximity to s -wave superconductor

T. Yu and M. W. Wu*

*Hefei National Laboratory for Physical Sciences at Microscale, Department of Physics,
and CAS Key Laboratory of Strongly-Coupled Quantum Matter Physics,
University of Science and Technology of China, Hefei, Anhui, 230026, China*

(Dated: September 16, 2021)

We show that the *gapped* triplet superconductivity, i.e., a triplet superconductor with triplet order parameter, can be realized in strong spin-orbit-coupled (100) quantum wells in proximity to s -wave superconductor. It is revealed that with the singlet order parameter induced from the superconducting proximity effect, in quantum wells, not only can the triplet pairings arise due to the spin-orbit coupling, but also the triplet order parameter can be induced due to the repulsive effective electron-electron interaction, including the electron-electron Coulomb and electron-phonon interactions. This is a natural extension of the work of de Gennes, in which the repulsive-interaction-induced singlet order parameter arises in the normal metal in proximity to s -wave superconductor [Rev. Mod. Phys. **36**, 225 (1964)]. Specifically, we derive the effective Bogoliubov-de Gennes equation, in which the self-energies due to the effective electron-electron interactions contribute to the singlet and triplet order parameters. It is further shown that for the singlet order parameter, it is efficiently suppressed due to this self-energy renormalization; whereas for the triplet order parameter, it is the p -wave ($p_x \pm ip_y$) one with the \mathbf{d} -vector parallel to the effective magnetic field due to the spin-orbit coupling. Finally, we perform the numerical calculation in InSb (100) quantum wells. Specifically, we reveal that the Coulomb interaction is much more important than the electron-phonon interaction at low temperature. Moreover, it shows that with proper electron density, the minimum of the renormalized singlet and the maximum of the induced triplet order parameters are comparable, and hence can be experimentally distinguished.

PACS numbers: 74.20.-z, 74.45.+c, 71.55.Eq, 71.70.Ej

I. INTRODUCTION

In recent years, triplet superconductivity has attracted much attention, which provides the possibility to realize the nondissipative spin transport and hence has potential application in spintronics.^{1–11} To confirm or realize the triplet superconductivity, much efforts have been made to several potential systems, including the unconventional superconductor Sr_2RuO_4 ,^{12–19} the conventional superconductor-ferromagnet (S-F) interface with induced odd-frequency and even-momentum triplet pairings,^{2–4,20–24} conventional superconductors with induced spin-orbit coupling (SOC) in the surface or interface which possess even-frequency and odd-momentum triplet pairings,^{20,25–30} and the non-centrosymmetric superconductors including the heavy fermion system.^{31–33}

Specifically, Sr_2RuO_4 was suggested to be the triplet p -wave superconductor which may arise from the spin-fluctuation-induced attractive potential between the triplet states,^{14,34–36} whose experimental confirmation is still in progress.^{12–19} In conventional S-F interface, it is shown that with the existence of the exchange field due to the ferromagnet, the spin-degeneracy is lifted. Accordingly, the odd-frequency and even-momentum triplet Cooper pairings emerge at the interface of S-F, in which the triplet order parameter is further shown to be zero.^{2–4,21–24,37} One notes that the order parameter directly contributes to the superconducting gap. Specifically, it is well established that with the inhomogeneous

ferromagnet, the induced triplet pairs can diffuse into the ferromagnetic materials over distances much larger than the singlet ones, which is referred to as long-range proximity effect.²² Similar to the exchange field, SOC can also lift the spin degeneracy and hence provides another possibility to realize the triplet superconductivity.^{25–28,30} This possibility was first pointed out by Gor'kov and Rashba when considering the s -wave superconductivity with the SOC induced by the absorption of ion.²⁵ It was shown that due to the lift of the spin-degeneracy by the SOC, mixed singlet-triplet Cooper pairings arise in which the triplet part is odd-momentum and even-frequency. We point out here that with the momentum-independent attractive potential between electrons from the s -wave channel, no triplet gap or triplet order parameter arises in the superconductor. As a natural extension, much efforts are focused on the system with the SOC in proximity to the s -wave superconductors, including spin-orbit-coupled metals^{22,26–29} and even semiconductors.³⁰ Finally, in the non-centrosymmetric superconductor, with the SOC naturally existing in the superconductor itself, it is shown that if proper forms of *attractive* effective electron-electron (e-e) interaction potential are realized from the symmetry analysis, triplet gap or triplet order parameter can be realized.^{31–33} Specifically, it is shown that when the \mathbf{d} -vector of the triplet order parameter is parallel to the effective magnetic field due to the SOC, the system can have minimum free energy.³²

In above systems, one can see that in Sr_2RuO_4 and

non-centrosymmetric superconductors, the triplet order parameter can naturally arise from proper effective e-e interaction potential.^{14,31,32} However, their experimental confirmations are still in progress.^{12-19,31,32} In contrast to this, the triplet superconductivity in the system with the Zeeman field or SOC,^{2-4,21-24,26-30} which is in proximity to the *s*-wave superconductor, is relatively easy to be realized and manipulated with the flexible manipulation of the strength and type of the SOC.³⁸⁻⁴⁰ Specifically, the triplet superconductivity in conventional S-F interface or the S-F-S Josephson junction has been experimentally confirmed by observing the structure of the energy gap^{23,24} or 0- π transition of Josephson effect.⁴¹⁻⁴⁴ Nevertheless, it is shown that although there exists triplet pairings, no triplet order parameter arises in both the interface of conventional S-F and the system with SOC in proximity to conventional *s*-wave superconductors.^{2-4,25} As a consequence, the elementary excitation spectra cannot be influenced by the triplet pairings, and are only determined by the singlet order parameter. Furthermore, in the interface of conventional S-F, in the ferromagnet side, when the singlet order parameter can be neglected due to the weak interaction potential, the system shows gapless structure.^{2,3,23,24,45} Due to the gapless structure, the experimental realization of the gapless triplet superconductivity is performed at extremely low temperature due to the absence of the gap protection.

One further notes that in above *metal* systems with the Zeeman field or SOC which are in proximity to the *s*-wave superconductors, the e-e interaction can be neglected due to the strong screening.²⁻⁴ Nevertheless, in the study of the boundary effects in superconductors-normal metal, de Gennes pointed out that the Cooper pairs tunneling or diffusing from the *s*-wave superconductor also experience the many-body interaction in the normal metal, in which the singlet order parameter can be induced even with a *repulsive* effective e-e interaction.⁴⁵ Accordingly, it is natural to consider the possibility to realize the triplet order parameter in system with the Zeeman field or SOC in proximity to the *s*-wave superconductor from the effective e-e interaction, which can protect the ground state and is promising to provide rich physics especially for the elementary excitation. As expected, this effect is significant only when the effective e-e interaction is strong. This can be realized in low-dimensional semiconductors with weak screening effect, based on the facts that the proximity-induced superconductivity from *s*-wave superconductor in two-dimensional (2D) electron gas, including InAs^{46,47} and GaAs⁴⁸⁻⁵⁰ heterostructures, and quantum nanowire⁵¹⁻⁵⁴ has been reported in the literature.

In the present work, we show that a *gapped* triplet superconductivity with triplet order parameter can be realized in 2D electron gas of the spin-orbit-coupled quantum wells (QWs) in proximity to the *s*-wave superconductor. This triplet order parameter is induced by the effective e-e interaction including the Coulomb and electron-phonon (e-p) interactions, even the total interactions are repulsive. Specifically, based on the superconducting prox-

imity effect, it has been shown that the singlet order parameter can be induced in the 2D electron gas.⁵⁵⁻⁵⁷ With this proximity-induced singlet order parameter, it can be further shown that the triplet pairings are induced due to the SOC.²⁵ Furthermore, we derive the effective Bogoliubov-de Gennes (BdG) equation, in which the self-energy due to the *momentum-dependent* e-e and e-p interactions is presented explicitly.⁵⁸⁻⁶⁰ Specifically, in the effective BdG equation, the self-energy from the effective e-e interaction leads to the *p*-wave ($p_x \pm ip_y$) triplet order parameter. Moreover, from the effective BdG equation, it is discovered that the proximity-induced singlet order parameter is also inevitably renormalized by the effective e-e interactions.

To make the physics clearer, we further carry out the numerical calculation in the specific material InSb (100) QWs, in which there exists strong SOC.^{61,62} The calculations show that the self-energy due to the e-p interaction is much smaller than that due to the e-e Coulomb interaction at low temperature ($T=2$ K), and hence only the Coulomb interaction needs to be considered here. For the renormalized singlet order parameter, it is always smaller than the proximity-induced one, as the renormalization from the Coulomb interaction is in the opposite sign against the proximity-induced order parameter. Moreover, it is shown that it only depends on the magnitude of the momentum, and decreases with the increase of the energy due to the suppression of the Coulomb interaction at high energy. For the induced triplet order parameter, it depends not only on the magnitude of the momentum, but also on its angle. Specifically, in the momentum-module dependence, a *peak* is predicted from our theory. In the angular dependence, it is proved that the **d**-vector of this triplet order parameter is parallel to the effective magnetic field due to the SOC, and hence is protected by the SOC.³² Finally, we study the electron density dependencies of the singlet and triplet order parameters in detail. Rich behaviors arise when the electrons populate different energy bands, which are split by the strong SOC. It is further found that with proper electron density ($n_e \approx 8 \times 10^{14} \text{ cm}^{-2}$), the minimum of the renormalized singlet order parameter and the maximum of the induced triplet order parameter are comparable, which provides an ideal condition to observe and distinguish these order parameters in the experiment.

This paper is organized as follows. In Sec. II, we set up the model and Hamiltonian. In Sec. III, we present the analytical results including the effective BdG equation (Sec. III A) and the calculation of the e-e and e-h self-energies (Sec. III B). In Sec. IV, the numerical results are performed in InSb (100) QWs, in which both the suppression of the proximity-induced singlet order parameter (Sec. IV A) and induced triplet order parameter (Sec. IV B) are discussed. We summarize and discuss in Sec. V.

II. MODEL AND HAMILTONIAN

We start our investigation from the Hamiltonian of the (100) *symmetric* QWs in proximity to the *s*-wave superconductor, which is composed by the Hamiltonian of (100) QWs \hat{H}_{QW} (Sec. II A) and the Hamiltonian of the *s*-wave superconductor \hat{H}_{S} (Sec. II B).

A. Hamiltonian of (100) QWs

The Hamiltonian of (100) QWs is written as

$$\hat{H}_{\text{QW}} = \hat{H}_{\text{QW}}^{\text{k}} + \hat{H}_{\text{QW}}^{\text{soc}} + \hat{H}_{\text{QW}}^{\text{ee}} + \hat{H}_{\text{QW}}^{\text{ep}}. \quad (1)$$

Here, $\hat{H}_{\text{QW}}^{\text{k}}$, $\hat{H}_{\text{QW}}^{\text{soc}}$, $\hat{H}_{\text{QW}}^{\text{ee}}$ and $\hat{H}_{\text{QW}}^{\text{ep}}$ are the kinetic energy of the electron, the SOC, the e-e Coulomb interaction and e-p interaction, respectively. In QWs, by using the field operator defined in Nambu \otimes spin space $\hat{\Psi}(\mathbf{r}) = (\psi_{\uparrow}(\mathbf{r}), \psi_{\downarrow}(\mathbf{r}), \psi_{\uparrow}^{\dagger}(\mathbf{r}), \psi_{\downarrow}^{\dagger}(\mathbf{r}))^T$, these Hamiltonians are given as follows. The kinetic energy reads ($\hbar \equiv 1$ throughout this paper)

$$\hat{H}_{\text{QW}}^{\text{k}} = \frac{1}{2} \int d\mathbf{r} \hat{\Psi}^{\dagger}(\mathbf{r}) (\varepsilon_{\mathbf{k}} - \mu) \hat{\tau}_3 \hat{\Psi}(\mathbf{r}), \quad (2)$$

where $\varepsilon_{\mathbf{k}} = \mathbf{k}^2/(2m^*)$ with $\mathbf{k} = (k_x, k_y)$ being the momentum of electron, m^* denotes the effective mass of electron, μ represents the chemical potential, and $\hat{\tau}_3 = \text{diag}(1, 1, -1, -1)$. The SOC Hamiltonian is

$$\hat{H}_{\text{QW}}^{\text{soc}} = \frac{1}{2} \int d\mathbf{r} \hat{\Psi}^{\dagger}(\mathbf{r}) \begin{pmatrix} \hat{h}_{\text{soc}}(\hat{\mathbf{k}}) & 0 \\ 0 & \hat{h}_{\text{soc}}^*(-\hat{\mathbf{k}}) \end{pmatrix} \hat{\tau}_3 \hat{\Psi}(\mathbf{r}). \quad (3)$$

Here, $\hat{h}_{\text{soc}}(\mathbf{k}) = -\alpha \hat{k}_x \sigma_x + \alpha \hat{k}_y \sigma_y$ in which $\alpha = \gamma_D(\pi/a)^2$ for the infinitely deep well with γ_D and a being the Dresselhaus coefficient and well width, respectively, and $\sigma = (\sigma_x, \sigma_y, \sigma_z)$ are the Pauli matrices.^{63,64}

The e-e Hamiltonian is written as

$$\hat{H}_{\text{QW}}^{\text{ee}} = \frac{1}{2} \int d\mathbf{r} d\mathbf{r}' V(\mathbf{r}-\mathbf{r}') [\hat{\Psi}^{\dagger}(\mathbf{r}) \hat{\tau}_3 \hat{\Psi}(\mathbf{r})] [\hat{\Psi}^{\dagger}(\mathbf{r}') \hat{\tau}_3 \hat{\Psi}(\mathbf{r}')], \quad (4)$$

where $V(\mathbf{r} - \mathbf{r}')$ denotes the screened Coulomb potential, whose Fourier transformation is represented by $V(\mathbf{k}) = \frac{V_0(\mathbf{k})}{1 - P^{(1)}(\mathbf{k})V_0(\mathbf{k})}$. Here, $V_0(\mathbf{k}) =$

$\int dy \frac{1}{\pi a \varepsilon_0 \kappa_0 (k^2 + 4y^2/a^2)} |I(y)|^2$ with ε_0 and κ_0 standing for the vacuum permittivity and relative dielectric constant; $|I(y)|^2 = \frac{\pi^4 \sin^2(y)}{(\pi^2 - y^2)^2 y^2}$ representing the form factor; $P^{(1)}(\mathbf{k})$ denoting the longitudinal polarization function, whose expression is derived based on the linear-response theory with density-density correlation function (refer to Appendix. B).^{58-60,65}

Finally, the e-p interaction Hamiltonian is denoted as

$$\hat{H}_{\text{QW}}^{\text{ep}} = \frac{1}{2} \int d\mathbf{r} d\mathbf{r}' g(\mathbf{r} - \mathbf{r}') \hat{\Psi}^{\dagger}(\mathbf{r}) \hat{\tau}_3 \hat{\Psi}(\mathbf{r}) \phi(\mathbf{r}'), \quad (5)$$

where $g(\mathbf{r} - \mathbf{r}')$ is the coupling potential between electron and phonon and $\phi(\mathbf{r})$ is the phonon field operator. Specifically, at low temperature, we focus on three electron-AC-phonon interactions due to the deformation potential in LA-branch and piezoelectric coupling including LA and TA branches. The Fourier transformations of the coupling potential $g(\mathbf{r} - \mathbf{r}')$ between the AC phonons and electrons are explicitly given in Refs. 63,66.

B. Hamiltonian of *s*-wave superconductor

In the conventional *s*-wave superconductor, with the field operator in Nambu \otimes spin space expressed as $\hat{\Phi}(\mathbf{r}) = (\phi_{\uparrow}(\mathbf{r}), \phi_{\downarrow}(\mathbf{r}), \phi_{\uparrow}^{\dagger}(\mathbf{r}), \phi_{\downarrow}^{\dagger}(\mathbf{r}))^T$, the Hamiltonian is expressed as

$$\hat{H}_{\text{S}} = \frac{1}{2} \int d\mathbf{r} \hat{\Phi}^{\dagger}(\mathbf{r}) \hat{H}_{\text{S}}^{\text{BdG}} \hat{\Phi}(\mathbf{r}), \quad (6)$$

where the BdG Hamiltonian $\hat{H}_{\text{S}}^{\text{BdG}}$ is written as

$$\hat{H}_{\text{S}}^{\text{BdG}} = \begin{pmatrix} \frac{\hat{\mathbf{p}}^2}{2\tilde{m}} - \tilde{\mu} & 0 & 0 & -\Delta_0 \\ 0 & \frac{\hat{\mathbf{p}}^2}{2\tilde{m}} - \tilde{\mu} & \Delta_0 & 0 \\ 0 & -\Delta_0^* & \frac{\hat{\mathbf{p}}^2}{2\tilde{m}} - \tilde{\mu} & 0 \\ \Delta_0^* & 0 & 0 & \frac{\hat{\mathbf{p}}^2}{2\tilde{m}} - \tilde{\mu} \end{pmatrix} \hat{\tau}_3. \quad (7)$$

In Eq. (7), for the electron in the superconductor, $\mathbf{p} = (p_x, p_y, p_z)$ is the momentum; \tilde{m} and $\tilde{\mu}$ are the mass and chemical potential, respectively; and Δ_0 denotes the singlet gap, which is taken to be real in this work.

III. ANALYTICAL RESULTS

A. Effective BdG equation in QWs

In this section, we derive the effective BdG equation in QWs by using the equilibrium Green function method in the Matsubara representation in the Nambu \otimes spin space, from which we obtain that the self-energies due to the effective e-e interactions act as the effective singlet and triplet pairing potentials (order parameters).⁵⁸⁻⁶⁰ Here, the zeroth-order Hamiltonian is chosen to be $\hat{H}_{\text{QW}}^0 = \hat{H}_{\text{QW}}^{\text{k}} + \hat{H}_{\text{QW}}^{\text{soc}}$, and $\hat{H}_{\text{QW}}^{\text{ee}}$ and $\hat{H}_{\text{QW}}^{\text{ep}}$ are treated as perturbations. In the Nambu \otimes spin space, the equilibrium Green function is defined as

$$G_{12} = -\hat{\tau}_3 \langle T_{\tau} \hat{\Psi}_1 \hat{\Psi}_2^{\dagger} \rangle, \quad (8)$$

with T_{τ} representing the chronological product, $(1) = (\tau_1, \mathbf{r}_1)$ representing the imaginary-time-space point, and $\langle \dots \rangle$ denoting the ensemble average.⁵⁸⁻⁶⁰

When no interactions are included, the eigenstates of \hat{H}_{QW}^0 are expressed as the spinor wavefunction $U_n(\mathbf{r}) = (u_{n,\uparrow}(\mathbf{r}), u_{n,\downarrow}(\mathbf{r}), v_{n,\uparrow}(\mathbf{r}), v_{n,\downarrow}(\mathbf{r}))^T$ for the

n th-state with eigen-energy E_n , i.e., $\hat{H}_{\text{QW}}^0 U_n(\mathbf{r}) = E_n U_n(\mathbf{r})$. For these eigenstates, the orthonormal conditions $\int d\mathbf{r} U_n^\dagger(\mathbf{r}) U_{n'}(\mathbf{r}) = \delta_{nn'}$ and $\sum_n U_n(\mathbf{r}) U_n^\dagger(\mathbf{r}') = \delta(\mathbf{r} - \mathbf{r}')$ are satisfied. Accordingly, the field operator in the Heisenberg representation can be expanded by these eigenstates as $\Psi^\dagger(\tau, \mathbf{r}) = \sum_n e^{E_n \tau} U_n^\dagger(\mathbf{r}) \alpha_n^\dagger$, where α_n^\dagger is the creation operator for n th state. Accordingly, from Eq. (8), the free Green function is represented as

$$G_{12}^0 = - \sum_n \hat{\tau}_3 U_n(\mathbf{r}_1) U_n^\dagger(\mathbf{r}_2) e^{-E_n(\tau_1 - \tau_2)} \times \left[\theta(\tau_1 - \tau_2) \langle \alpha_n \alpha_n^\dagger \rangle - \theta(\tau_2 - \tau_1) \langle \alpha_n^\dagger \alpha_n \rangle \right], \quad (9)$$

where $\theta(\tau_1 - \tau_2)$ is the Heaviside step function. Then from Eq. (9), one can obtain the dynamics equation for the free Green function,

$$\left(-\frac{\partial}{\partial \tau_1} \hat{\tau}_3 - \hat{H}_{\text{QW}}^0 \hat{\tau}_3 \right) G_{12}^0 = \delta(1 - 2). \quad (10)$$

In the Matsubara-frequency space, $G^0(\mathbf{r}_1, \mathbf{r}_2; i\omega_m) = \int_0^\beta d\tau e^{i\omega_m \tau} G^0(\mathbf{r}_1, \mathbf{r}_2; \tau)$, where $\beta = 1/(k_B T)$ and $\omega_m = (2m + 1)\pi/\beta$ are Matsubara frequencies with m being integer. Then in this space, Eq. (10) is transformed into

$$(i\omega_m \hat{\tau}_3 - \hat{H}_{\text{QW}}^0 \hat{\tau}_3) G^0(\mathbf{r}_1, \mathbf{r}_2; i\omega_m) = \delta(\mathbf{r}_1 - \mathbf{r}_2). \quad (11)$$

When the interactions are considered, the eigenfunction and creation (annihilation) operator are expressed as \tilde{U}_n and $\tilde{\alpha}_n^\dagger$ ($\tilde{\alpha}_n$), respectively, whose eigen-energy is \tilde{E}_n . Accordingly, the Green function in Matsubara-frequency space is expressed as

$$G(\mathbf{r}_1, \mathbf{r}_2; i\omega_m) = \sum_n \hat{\tau}_3 \tilde{U}_n(\mathbf{r}_1) \tilde{U}_n^\dagger(\mathbf{r}_2) \frac{1}{i\omega_m - \tilde{E}_n}. \quad (12)$$

From the Dyson equation, one can also express the above Green function as

$$G(\mathbf{r}_1, \mathbf{r}_2; i\omega_m) = G^0(\mathbf{r}_1, \mathbf{r}_2; i\omega_m) + \int d\mathbf{r}_3 d\mathbf{r}_4 G^0(\mathbf{r}_1, \mathbf{r}_3; i\omega_m) \times \Sigma(\mathbf{r}_3, \mathbf{r}_4; i\omega_m) G(\mathbf{r}_4, \mathbf{r}_2; i\omega_m), \quad (13)$$

where $\Sigma(\mathbf{r}_3, \mathbf{r}_4; i\omega_m)$ are the self-energies due to $\hat{H}_{\text{QW}}^{\text{ee}}$ and $\hat{H}_{\text{QW}}^{\text{ep}}$. By performing the operation $(i\omega_m \hat{\tau}_3 - \hat{H}_{\text{QW}}^0 \hat{\tau}_3)$ on Eq. (13), with Eq. (11), one obtains

$$\hat{H}_{\text{QW}}^0 \tilde{U}_n(\mathbf{r}) + \int d\mathbf{r}' \Sigma(\mathbf{r} - \mathbf{r}', i\omega_m) \hat{\tau}_3 \tilde{U}_n(\mathbf{r}') = \tilde{E}_n \tilde{U}_n(\mathbf{r}). \quad (14)$$

Specifically, in homogeneous space, Eq. (14) is written in the momentum-space as

$$[\hat{H}_{\text{QW}}^0(\mathbf{k}) + \Sigma(\mathbf{k}, i\omega_m) \hat{\tau}_3] \tilde{U}_n(\mathbf{k}) = \tilde{E}_n(\mathbf{k}) \tilde{U}_n(\mathbf{k}). \quad (15)$$

Finally, in the real-frequency space, by using the analytical continuation $i\omega_m \rightarrow \omega + i0^+$, Eq. (15) becomes

$$[\hat{H}_{\text{QW}}^0(\mathbf{k}) + \Sigma(\mathbf{k}, \omega) \hat{\tau}_3] \tilde{U}_n(\mathbf{k}) = \tilde{E}_n(\mathbf{k}) \tilde{U}_n(\mathbf{k}). \quad (16)$$

Eq. (16) is the *effective BdG equation* in QWs, which can be used to calculate the energy-spectra and wavefunction of the elementary excitation. Moreover, from the structure of the self-energy $\Sigma(\mathbf{k}, i\omega_m)$, one can obtain the effective singlet and triplet order parameters, which are presented in Sec. III B 1 and III B 2, respectively.

B. Singlet and triplet order parameters from self-energy

In this part, we present the self-energies due to the superconducting proximity effect, e-e and e-p interactions, respectively. One notes that the self-energies and Green function should be calculated consistently, because the Green function determines the self-energy and vice versa, from Eq. (13), the self-energy also influences the Green function. Therefore, when there exists two kinds of self-energies, i.e., the self-energy due to the superconducting proximity effect and the self-energy due to e-e and e-p interactions, their calculations are complicated because they are influenced on each other through the determination of the Green function. However, when the two kinds of interactions are not comparable, the calculation is highly simplified. Here, the e-e and e-p interactions are weaker than the one due to superconducting proximity effect. This makes it reasonable to calculate the self-energy due to the superconducting proximity effect without consideration of the e-e and e-p interactions, from which the Green function including the superconducting proximity effect is determined (Sec. III B 1). With this Green function, we further calculate the self-energy due to e-e and e-p interactions (Sec. III B 2).

1. Self-energy and Green function due to superconducting proximity effect

In this part, the self-energy and Green function due to the superconducting proximity effect are presented. Specifically, the self-energy due to the superconducting proximity effect is written as

$$\Sigma_s(\bar{k}) \approx \begin{pmatrix} 0 & 0 & 0 & -\Delta(\bar{k}) \\ 0 & 0 & \Delta(\bar{k}) & 0 \\ 0 & -\Delta^*(\bar{k}) & 0 & 0 \\ \Delta^*(\bar{k}) & 0 & 0 & 0 \end{pmatrix}, \quad (17)$$

where $\bar{k} \equiv (i\omega_m, \mathbf{k})$. Here, from Eqs. (15) and (16), one observes that $\Delta(\bar{k})$ acts as the singlet order parameter in the QWs, which is referred to as proximity-induced singlet order parameter in this work. One notices that this self-energy [Eq. (17)] can be induced from the single-particle tunneling between QWs and superconductors (refer to Appendix A)^{55,56,67} and other possibilities.^{3,68}

From Eq. (17), we calculate the Green function for the 2D electron gas in QWs with the proximity-induced singlet order parameter included, based on the Dyson's

equation in frequency-momentum space,

$$G(\bar{k}) = G_0(\bar{k}) + G_0(\bar{k})\Sigma_s(\bar{k})G(\bar{k}). \quad (18)$$

By expressing

$$G(\bar{k}) = \begin{pmatrix} G_{\uparrow\uparrow}(\bar{k}) & G_{\uparrow\downarrow}(\bar{k}) & F_{\uparrow\uparrow}(\bar{k}) & F_{\uparrow\downarrow}(\bar{k}) \\ G_{\downarrow\uparrow}(\bar{k}) & G_{\downarrow\downarrow}(\bar{k}) & F_{\downarrow\uparrow}(\bar{k}) & F_{\downarrow\downarrow}(\bar{k}) \\ F_{\uparrow\uparrow}^*(-\bar{k}) & F_{\uparrow\downarrow}^*(-\bar{k}) & G_{\uparrow\uparrow}^*(-\bar{k}) & G_{\uparrow\downarrow}^*(-\bar{k}) \\ F_{\downarrow\uparrow}^*(-\bar{k}) & F_{\downarrow\downarrow}^*(-\bar{k}) & G_{\downarrow\uparrow}^*(-\bar{k}) & G_{\downarrow\downarrow}^*(-\bar{k}) \end{pmatrix}, \quad (19)$$

one obtains the normal Green function

$$\begin{pmatrix} G_{\uparrow\uparrow}(\bar{k}) & G_{\uparrow\downarrow}(\bar{k}) \\ G_{\downarrow\uparrow}(\bar{k}) & G_{\downarrow\downarrow}(\bar{k}) \end{pmatrix} = \frac{1}{2} \begin{pmatrix} A_+(\bar{k}) + A_-(\bar{k}) & h_{\mathbf{k}}[A_+(\bar{k}) - A_-(\bar{k})] \\ h_{\mathbf{k}}^*[A_+(\bar{k}) - A_-(\bar{k})] & A_+(\bar{k}) + A_-(\bar{k}) \end{pmatrix}, \quad (20)$$

and anomalous (Gor'kov's) Green function⁶⁰

$$\begin{pmatrix} F_{\uparrow\uparrow}(\bar{k}) & F_{\uparrow\downarrow}(\bar{k}) \\ F_{\downarrow\uparrow}(\bar{k}) & F_{\downarrow\downarrow}(\bar{k}) \end{pmatrix} = \frac{1}{2} \begin{pmatrix} h_{\mathbf{k}}[B_-(\bar{k}) - B_+(\bar{k})] & B_+(\bar{k}) + B_-(\bar{k}) \\ -B_+(\bar{k}) - B_-(\bar{k}) & h_{\mathbf{k}}^*[B_+(\bar{k}) - B_-(\bar{k})] \end{pmatrix}. \quad (21)$$

In Eqs. (20) and (21), $A_{\pm}(\bar{k}) = \frac{i\omega_m + \epsilon_{\mathbf{k}\pm}}{(i\omega_m)^2 - \epsilon_{\mathbf{k}\pm}^2 - |\Delta(\bar{k})|^2}$ and $B_{\pm}(\bar{k}) = \frac{\Delta(\bar{k})}{(i\omega_m)^2 - \epsilon_{\mathbf{k}\pm}^2 - |\Delta(\bar{k})|^2}$ with $\epsilon_{\mathbf{k}\pm} = \frac{k^2}{2m^*} \pm \alpha k - \mu = E_{k,\pm} - \mu$; $h_{\mathbf{k}} = -e^{i\phi_{\mathbf{k}}}$ with $\phi_{\mathbf{k}}$ being the angle of the momentum.

Some features can be revealed from the normal and anomalous Green functions [Eqs. (20) and (21)] when there exists the SOC. Specifically, from the off-diagonal terms of the normal Green function [Eq. (20)], one concludes that there always exists correlation for the electron with different spins due to the SOC. From the anomalous Green function [Eq. (21)], there exist anomalous correlations for the electrons not only with the same spins, i.e., the off-diagonal terms in Eq. (21), but also with different spins, i.e., the diagonal terms in Eq. (21). Therefore, one can realize the mixed singlet-triplet pairings in spin-orbit-coupled QWs in proximity to conventional *s*-wave superconductors.²⁵ Nevertheless, from the effective BdG equation with the self-energy due to the superconducting proximity effect, i.e., Eq. (16), one can see that only the singlet component contributes the order parameter. In the following, we can show that when the e-e and e-p interactions are further considered, the triplet order parameter is also induced and hence the gapped triplet superconductivity can be realized.

2. Self-energy due to e-e and e-p interactions

In this part, the self-energies due to e-e and e-p interactions are derived, whose Feynman diagram is shown in

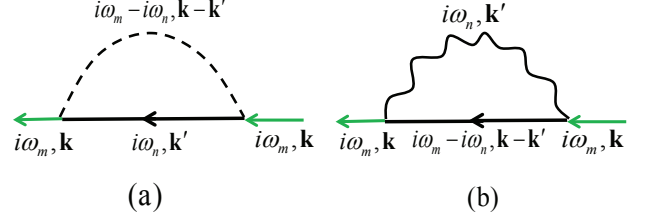


FIG. 1: (Color online) Feynman diagrams for the calculation of self-energies due to e-e [(a)] and e-p [(b)] interactions. Here, \leftarrow represents the Green function $G(i\omega_m, \mathbf{k})$ [Eq. (19)] in matrix form. The black dashed curve in (a) and black wavy curve in (b) represent the Coulomb potential and phonon Green function, respectively.

Figs. 1(a) and (b), respectively. For the e-e interaction, from the Feynman diagram in Fig. 1(a), the self-energy in the Matsubara representation is written as

$$\Sigma_{ee}(\mathbf{k}) = -\frac{1}{\beta} \int \frac{d\mathbf{k}'}{(2\pi)^2} V(\mathbf{k} - \mathbf{k}') \sum_n G(i\omega_n, \mathbf{k}'). \quad (22)$$

For the e-p interaction, from the Feynman diagram in Fig. 1(b), the self-energy reads

$$\Sigma_{ep}(i\omega_m, \mathbf{k}) = -\frac{1}{\beta} \sum_n \int \frac{d\mathbf{k}'}{(2\pi)^2} \int \frac{dq_z}{2\pi} |g_{\mathbf{k}', q_z}|^2 \times \frac{2\omega_{\mathbf{k}', q_z}}{(i\omega_n)^2 - \omega_{\mathbf{k}', q_z}^2} G(i\omega_m - i\omega_n, \mathbf{k} - \mathbf{k}'). \quad (23)$$

In Eq. (23), $g_{\mathbf{k}', q_z}$ denote the e-p interactions due to the deformation potential (LA-branch) and piezoelectric coupling (LA and TA branches), and $\omega_{\mathbf{k}, q_z}$ are the corresponding energy spectra. For LA and TA phonons, $\omega_{\mathbf{k}, q_z}^{sl} = v_{sl} \sqrt{k^2 + q_z^2}$ and $\omega_{\mathbf{k}, q_z}^{st} = v_{st} \sqrt{k^2 + q_z^2}$, respectively, with v_{sl} and v_{st} being the velocities of LA and TA phonons, respectively.^{63,66}

From the structure of the self-energies due to the e-e and e-p interactions, one observes that every elements in these 4×4 matrices are renormalized, including the effective mass, the zero-energy point, the strength of the SOC and the singlet order parameter. Specifically, the triplet order parameter is induced due to the existence of the triplet pairings. Here, we neglect the renormalization of the effective mass, the zero-energy point and the SOC strength (which is shown to be negligible compared to the original SOC), and focus on the renormalization of the singlet and induction of the triplet order parameters, whose concrete analytical expressions and numerical values are discussed in detail in Sec. IV.

IV. NUMERICAL RESULTS

In this section, to show the physics more clearly and quantitatively, we numerically calculate the self-energies

due to the e-e and e-p interactions based on Eqs. (22) and (23). We choose the material with strong SOC: i.e., InSb (100) QWs. All parameters including the band structure and material parameters used in our computation are listed in Table I.^{61,62}

TABLE I: Parameters used in the computation for self-energies due to the e-e and e-p interactions.^{61,62}

m^*/m_0	0.015	n_0 (cm ⁻²)	10 ¹⁴
κ_0	16.0	γ_D (eV · Å ³)	389
κ_∞	15.68	a (nm)	3
d (kg/cm ³)	5.8	T (K)	2
Ξ (eV)	14.5	v_{sl} (m/s)	3770
e_{14} (10 ⁹ V/m)	1.41	v_{st} (m/s)	1630

In Table I, d is the mass density of the crystal; Ξ denotes the deformation potential; and e_{14} represents the piezoelectric constant. In our computation, the electron densities n_e in QWs vary from n_0 to $35n_0$. With these electron densities, the chemical potential is calculated with the strong SOC explicitly included in the energy spectra by solving the equation

$$n_\uparrow = n_\downarrow = \frac{1}{2} \int \frac{d\mathbf{k}}{(2\pi)^2} [n_F(\epsilon_{\mathbf{k}+}) + n_F(\epsilon_{\mathbf{k}-})]. \quad (24)$$

In Eq. (24), n_\uparrow and n_\downarrow represent the electron densities with spin-up and spin-down, respectively; $n_F(\epsilon_{\mathbf{k}\pm}) = \left\{ \exp[\beta(\epsilon_{\mathbf{k}\pm} - \mu)] + 1 \right\}^{-1}$ is the Fermi-Dirac distribution function. Furthermore, in our computation, we focus on the *weak coupling limit* addressed in Refs. 55,56,67 with $|\Delta(\omega, \mathbf{k})| \ll \Delta_0$, where Δ_0 is one to several meV in conventional superconductors. Moreover, we focus on the low temperature limit. With these two conditions, one observes that the main physics happens in the regime $|\omega| \lesssim |\Delta(\omega, \mathbf{k})|$, and hence the frequency is much smaller than Δ_0 . In this situation, in the singlet order parameter due to the superconducting proximity effect, i.e., $\Delta(\omega, \mathbf{k})$ [Eq. (A7)], the frequency dependence can be neglected.^{55,56,67} Therefore, in our calculation, $\Delta(\omega, \mathbf{k})$ is set to be constant (0.5 meV) in the static approximation. It is emphasized that this approximation has little qualitative influence on the physics we reveal.^{55,56,67}

Finally, we point out that according to our calculation based on above parameters, it is found that the contribution of the self-energy mainly comes from the e-e interaction, as the contribution due to e-p interactions are two orders of magnitude smaller than that of the e-e interaction at low temperature. Accordingly, it is adequate to consider the e-e interaction here in the calculation and the following analysis.

A. Suppression of singlet order parameter

In this part, we focus on the calculation of the Coulomb-interaction-induced singlet order parameter $\Delta_s(\mathbf{k})$. From Eqs. (21) and (22), the Coulomb-interaction-induced singlet order parameter in the static approximation is obtained, which is written as

$$\Delta_s(\mathbf{k}) \approx -\frac{\Delta}{2\beta} \sum_{\mathbf{k}', n} \sum_{\eta=\pm} V_{\mathbf{k}-\mathbf{k}'} \frac{1}{\omega_n^2 + \epsilon_{\mathbf{k}'\eta}^2 + |\Delta|^2}. \quad (25)$$

One notes that according to Eq. (16), the Coulomb-interaction-induced order parameter is defined from the self-energy multiplying $\hat{\tau}_3$. From Eq. (25), one observes that $\Delta_s(\mathbf{k})$ always has opposite sign against the proximity-induced order parameter $\Delta(\omega = 0)$, because the summation in Eq. (25) is always positive with the repulsive e-e Coulomb interaction. This shows that the repulsive Coulomb interaction suppresses the singlet order parameter with the renormalized singlet order parameter $\Delta_S(\mathbf{k}) = \Delta + \Delta_s(\mathbf{k})$. It is further noted that this conclusion is consistent with the recent investigation in quantum nanowire in proximity to the *s*-wave superconductor, in which the Hubbard interaction is considered.⁶⁹

Furthermore, after the summation on the Matsubara frequencies, Eq. (25) becomes

$$\Delta_s(\mathbf{k}) = -\frac{m^*}{16\pi^2} \sum_{\eta=\pm} \int_0^\infty d\varepsilon_{\mathbf{k}'} d\phi_{\mathbf{k}'} F_{\mathbf{k}, \mathbf{k}'} \Lambda_\eta(\mathbf{k}') \times \left[1 - 2n_F(\sqrt{\epsilon_{\mathbf{k}'\eta}^2 + |\Delta|^2}) \right], \quad (26)$$

with $F_{\mathbf{k}, \mathbf{k}'} = V(\sqrt{k^2 + k'^2 - 2kk' \cos \phi_{\mathbf{k}'}})$, which is $\phi_{\mathbf{k}'}$ -independent, and $\Lambda_\pm(\mathbf{k}') = \Delta/\sqrt{\epsilon_{\mathbf{k}'\pm}^2 + |\Delta|^2}$. Accordingly, from Eq. (26), one observes that the renormalized singlet order parameter only depends on the magnitude of the momentum and is independent on its direction, which is calculated explicitly in the following.

1. Momentum dependence of the renormalized singlet order parameter

In this part, we study the momentum dependence of the renormalized singlet order parameter, which only depends on the magnitude of the momentum. In Fig. 2, the renormalized singlet order parameters $\Delta_S(\mathbf{k})$, shown by the green chain and yellow dashed curves for $n_e = 2n_0$ and $6n_0$, increase with the increase of the electron energy. This is because the magnitude of the Coulomb-interaction-induced singlet order parameters, i.e., $-\Delta_s(\mathbf{k})$, decreases with the increase of the electron energy for $n = 2n_0$ (the red solid curve with squares) and $6n_0$ (the blue dashed curve with squares), respectively. This can be understood from the fact that with the increase of the magnitude of the momentum and hence the electron energy, the Coulomb interaction is suppressed.

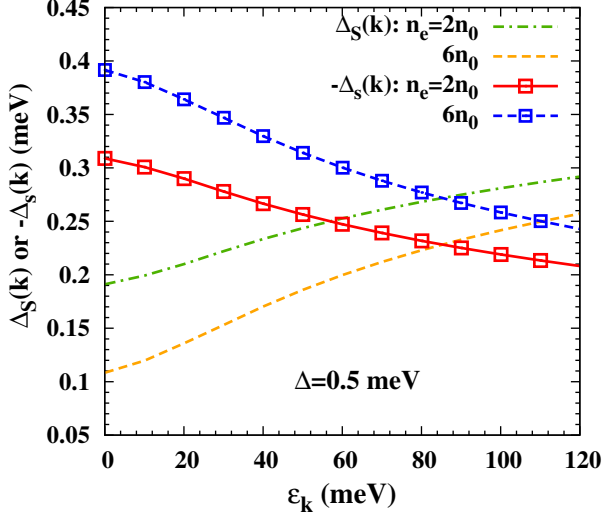


FIG. 2: (Color online) Energy-dependencies of the renormalized singlet order parameter $\Delta_S(\mathbf{k})$ and the magnitude of the Coulomb-interaction-induced singlet order parameter $-\Delta_S(\mathbf{k})$ with different electron densities $n = 2n_0$ and $6n_0$, respectively.

Furthermore, in Fig. 2, by observing the calculated results with $n_e = 2n_0$ and $6n_0$, one notices that the Coulomb-interaction-induced singlet order parameter and hence the renormalized singlet order parameter explicitly depends on the electron density in QWs. Actually, this provides a possible way to experimentally distinguish the singlet order parameter due to the superconducting proximity effect and that due to the e-e interaction. This is because the singlet order parameter due to the superconducting proximity effect marginally depends on the electron density in QWs [Eq. (A7)].

2. Electron density dependence of the Coulomb-interaction-induced singlet order parameter

In this part, we focus on the electron density dependence of the maximum of the Coulomb-interaction-induced singlet order parameter Δ_s^m at $\mathbf{k} = 0$. In Fig. 3, it is shown by the red solid curve with circles that with the increase of the electron density, Δ_s^m first shows a valley at relatively low electron density $n_e \approx 3n_0$, then a peak at the moderate electron density $n_e \approx 8n_0$, and finally decreases very slowly at high electron density $n_e \gtrsim 24n_0$. We first give the whole physics picture behind these rich and intriguing dependencies of Δ_s^m from the analysis of Eq. (25) when $\mathbf{k} = 0$.

From Eq. (25), one finds that with the increase of the electron density, both the Coulomb potential ($V_{\mathbf{k}'}$) and the proximity-induced singlet pairing ($\frac{1}{\omega_n^2 + \epsilon_{\mathbf{k}'\eta}^2 + |\Delta|^2}$)

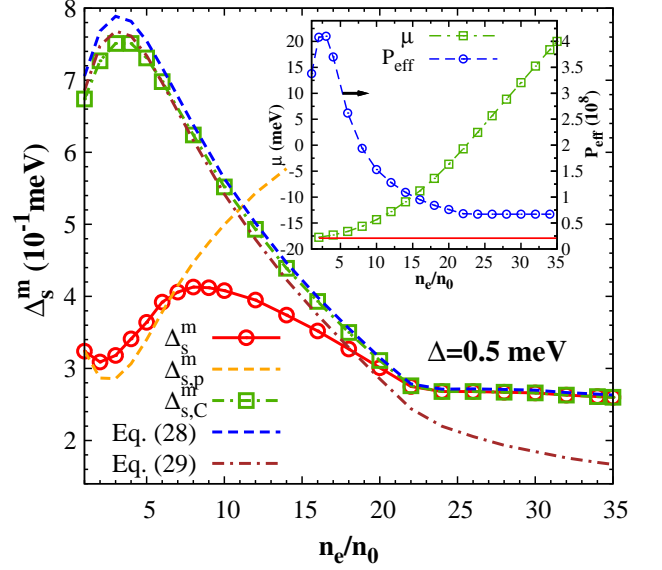


FIG. 3: (Color online) Density dependence of the maximum of the Coulomb-interaction-induced singlet order parameter Δ_s^m , shown by the red solid curve with circles. The yellow dashed curve (green chain curve with squares), labeled by $\Delta_{s,p}^m$ ($\Delta_{s,C}^m$), represents the maximum of the Coulomb-interaction-induced singlet order parameter when the proximity-induced singlet pairing (Coulomb potential) is arbitrarily taken to be independent on electron density. Furthermore, the blue dashed and purple chain curves denote the calculated results from Eqs. (28) and (29), respectively, in which the longitudinal polarization function is also taken to be constant. The inset zooms the density dependencies of the chemical potential and effective polarization function [Eq. (27)], in which the red solid line represents the band edge.

are varied due to their dependencies on the chemical potential, and hence both can influence of the electron density dependence of Δ_s^m . Specifically, in the inset of Fig. 3, it is shown by the blue dashed curve with circles that with the increase of the electron density, the effective polarization function

$$P_{\text{eff}} = e^2 / (\epsilon_0 \kappa_0) |P^{(1)}(\omega = 0, \mathbf{q} = 0)|. \quad (27)$$

shows a peak arising at the crossover between the non-degenerate and degenerate regimes with $n_e \approx 3n_0$, and becomes independent of the electron density when $n_e \gtrsim 20n_0$. Therefore, the strength of the Coulomb potential first decreases at low electron density and then increases at moderate one, and finally becomes independent of electron density at high electron density. As to the proximity-induced singlet pairing, with the increase of the electron density, it first varies slowly and then rapidly due to the electron density dependence of the chemical potential, which is shown by the green chain curve with squares in the inset of Fig. 3.

We find that the valley (decrease) in the electron density dependence of Δ_s^m at low (high) electron density comes from the electron density dependence of the

Coulomb potential (proximity-induced singlet pairing). This is confirmed from the fact that when the electron density is low (high), $\Delta_{s,p}^m$ ($\Delta_{s,C}^m$) with constant proximity-induced singlet pairing (constant Coulomb potential) at $n_e = n_0$ ($n_e = 35n_0$) almost coincides with Δ_s^m , shown by the yellow dashed curve (green chain curve with squares) in Fig. 3. Accordingly, at the moderate electron density $3n_0 \lesssim n_e \lesssim 20n_0$, with the increase of the electron density, the Coulomb potential tends to enhance Δ_s^m ; whereas the proximity-induced singlet pairing tends to suppress Δ_s^m . Thus, due to this competition of these two effects, a peak arises at the moderate electron density.

Nevertheless, one observes that for Δ_s^m and $\Delta_{s,p}^m$, there also exists small discrepancy for the value of the valley, with the former larger than the latter. This can be explained by the fact that when the Coulomb potential is set to be density independent, $\Delta_{s,C}^m$ shows a peak when $n_e \approx 3n_0$, which suppresses the value of valley. Moreover, although when $n_e \gtrsim 8n_0$, Δ_s^m decreases with the increase of the electron density, the rates of the decrease are drastically different for $8n_0 \lesssim n_e \lesssim 20n_0$ and $n_e \gtrsim 20n_0$. This can also be explained by the electron density dependence of $\Delta_{s,C}^m$, which decreases rapidly when $8n_0 \lesssim n_e \lesssim 20n_0$ and slowly when $n_e \gtrsim 20n_0$. Accordingly, a detailed physics picture can be obtained by analyzing the electron density dependence of $\Delta_{s,C}^m$, which is addressed as follows.

a. Single-band and double-band regimes To analyze the electron density dependence of $\Delta_{s,C}^m$, we first divide the system into different regimes according to the population of electrons with different chemical potentials. In the inset of Fig. 3, when $n_e \lesssim 3n_0$, the chemical potential is close to the band edge, which is shown by the red solid line, indicating that the system lies in the crossover between the non-degenerate and degenerate regimes. Moreover, when $n_e \lesssim 20n_0$, the chemical potential is negative, which shows that the electrons mainly populate at the $E_{\mathbf{k},-}$ -band; whereas when $n_e \gtrsim 20n_0$, $E_{\mathbf{k},+}$ -band becomes populated. To see this more clearly, in Fig. 4, the band structures for the $E_{\mathbf{k},-}$ and $E_{\mathbf{k},+}$ -bands are schematically plotted by the red and blue solid curves, respectively. In Fig. 4, the three situations mentioned above corresponding to $n_e \lesssim 3n_0$, $3n_0 \lesssim n_e \lesssim 20n_0$ and $n_e \gtrsim 20n_0$ are plotted by the dashed lines labeled by μ_1 , μ_2 and μ_3 , respectively. Accordingly, when $n_e \lesssim 20n_0$, only $E_{\mathbf{k},-}$ -band is efficiently populated, the system is referred to as *single-band regime*; whereas when $n_e \gtrsim 20n_0$, the $E_{\mathbf{k},+}$ -band becomes populated and the system is referred to as *double-band regime*.

b. Influence of proximity-induced singlet pairing in different regimes Before addressing the influence of the proximity-induced singlet pairing in different regimes, we first make some simplification in Eq. (26). One notes that when $\Delta \gg k_B T$ here, $n_F(\sqrt{\epsilon_{\mathbf{k}',\pm}^2 + |\Delta|^2}) \ll 1$ and hence can be neglected in Eq. (26). This is justified in Fig. 3 by the fact that when $n_F(\sqrt{\epsilon_{\mathbf{k}',\pm}^2 + |\Delta|^2})$ is not considered

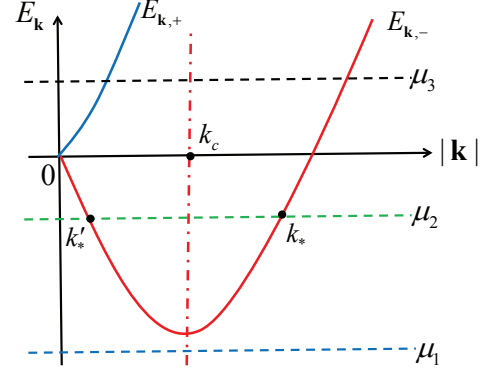


FIG. 4: (Color online) Schematic for the band structures of $E_{\mathbf{k},-}$ and $E_{\mathbf{k},+}$ -bands, shown by the red and blue solid curves, respectively. The dashed lines labeled by μ_1 , μ_2 and μ_3 correspond to the chemical potentials when $n_e \lesssim 3n_0$, $3n_0 \lesssim n_e \lesssim 20n_0$ and $n_e \gtrsim 20n_0$, respectively. k_c is the momentum corresponding to the band edge of $E_{\mathbf{k},-}$ -band; k_* and k'_* label the intersection points between μ_2 and $E_{\mathbf{k},-}$ -band with $k_* > k_c$ and $k'_* < k_c$, respectively.

in Eq. (26), $\Delta_{s,C}^m$ shown by the blue dashed curve almost coincides with the green chain curve with squares. In this situation, Eq. (26) with $\mathbf{k} = 0$ is simplified to be

$$\Delta_{s,C}^m \approx \frac{m^*}{8\pi} \int_0^\infty d\varepsilon_{\mathbf{k}'} F_{\mathbf{k}'}^* [\Lambda_-(\mathbf{k}') + \Lambda_+(\mathbf{k}')], \quad (28)$$

where $F_{\mathbf{k}'}^* = V_{\mathbf{k}=0,\mathbf{k}'}$ with polarization function taken to be the one when $n_e = 35n_0$. Nevertheless, one further notes that when $n_e \lesssim 20n_0$, only the $E_{\mathbf{k},-}$ -band is efficiently populated and hence $|\epsilon_{\mathbf{k},-}| \ll |\epsilon_{\mathbf{k},+}|$. Accordingly, Eq. (28) is further reduced to

$$\Delta_{s,C}^m \approx \frac{m^*}{8\pi} \int_0^\infty d\varepsilon_{\mathbf{k}'} F_{\mathbf{k}'}^* \Lambda_-(\mathbf{k}'). \quad (29)$$

Eq. (29) is justified in Fig. 3 with the fact that when $n_e \lesssim 20n_0$, $\Delta_{s,C}^m$ shown by the purple chain curve almost coincides with the blue dashed one.

When the system lies in the single-band (double-band) regime when $n_e \lesssim 20n_0$ ($n_e \gtrsim 20n_0$), the electron density dependence of $\Delta_{s,C}^m$ can be analyzed based on Eq. (29) [Eq. (28)]. Specifically, in the single-band regime, when $n_e \lesssim 3n_0$, the kinetic energy of electrons is larger than the chemical potential (refer to the inset in Fig. 3). In this situation, with the increase of the electron density and hence the chemical potential, $\epsilon_{\mathbf{k}',-}^2$ decreases, leading to the increase of $\Delta_{s,C}^m$ from Eq. (29). Whereas when $3n_0 \lesssim n_e \lesssim 20n_0$, the chemical potential is larger than the band edge. This situation is represented in Fig. 4 with the chemical potential μ_2 intersecting with the $E_{\mathbf{k},-}$ -band by two points k_* and k'_* . Specifically, $k_* > k_c$ and $k'_* < k_c$ with k_c being the momentum corresponding to the band edge of $E_{\mathbf{k},-}$ -band. From Eq. (29), one observes that when $\epsilon_{\mathbf{k},-} = 0$, $\Lambda_-(\mathbf{k})$ is the largest,

which means that the electrons around the chemical potential play the most important role in the renormalization of the singlet order parameter. For these electrons, with the increase of the chemical potential μ_2 , k_* increases and k'_* decreases. Nevertheless, k'_* is relatively small and can be even smaller than the wave-vector due to the effective polarization function, which cannot cause efficient variation of the Coulomb potential. Whereas the increase of k_* can efficiently suppress the Coulomb potential, and hence $\Delta_{s,C}^m$ decreases with the increase of the electron density in this regime. Furthermore, when $n_e \gtrsim 20n_0$, the system enters into the double-band regime, in which the $E_{\mathbf{k},+}$ -band becomes populated. Therefore, with the increase of the population of these electrons, the contribution of the $E_{\mathbf{k},+}$ -band to $\Delta_{s,C}^m$ increases with the increase of the electron density [Eq. (28)]. This tends to suppress the decrease of $\Delta_{s,a}^m$ due to the $E_{\mathbf{k},-}$ -band. Consequently, in this regime, $\Delta_{s,C}^m$ decreases very slowly with the increase of the electron density.

c. Summary of the physics picture By knowing the separate roles of the Coulomb potential and proximity-induced singlet pairing in the density dependence of Δ_s^m , the whole physics picture can be obtained. At the low electron density $n_e \lesssim 3n_0$, from the inset of Fig. 3, one observes that the polarization function varies rapidly, whereas the chemical potential varies slowly. In this situation, the influence of the Coulomb potential on the renormalized singlet order parameter is dominant. As a consequence, at the crossover of the non-degenerate and degenerate regimes with $n_e \approx 3n_0$, there exists a valley in the electron density dependence of Δ_s^m due to the dependence of the screening effect on electron density. Nevertheless, at the moderate electron density $3n_0 \lesssim n_e \lesssim 20n_0$, the screening effect tends to enhance Δ_s^m ; whereas the population of the electron in $E_{\mathbf{k},-}$ -band tends to suppress it. Thus, due to this competition of the two effects, a peak arises in the electron density dependence of the Δ_s^m . Finally, at the high electron density $n_e \gtrsim 20n_0$, from the inset of Fig. 3, one obtains that the effective polarization function becomes constant, whereas the chemical potential increases rapidly. Therefore, Δ_s decreases slowly due to the competition of the populations of electrons in $E_{\mathbf{k},+}$ and $E_{\mathbf{k},-}$ -bands.

B. Induced triplet p -wave order parameter

In this subsection, we discuss the triplet order parameter induced by the e-e Coulomb interaction. Specifically, from Eqs. (21) and (22), the induced triplet order parameter reads

$$\Delta_t(\mathbf{k}) = \begin{pmatrix} Q_-(\mathbf{k}) - Q_+(\mathbf{k}) & 0 \\ 0 & Q_+^*(\mathbf{k}) - Q_-^*(\mathbf{k}) \end{pmatrix}. \quad (30)$$

with

$$Q_{\pm}(\mathbf{k}) = \frac{m^*}{8\pi^2} e^{i\phi_{\mathbf{k}}} \int d\varepsilon_{\mathbf{k}'} d\phi_{\mathbf{k}'} \cos \phi_{\mathbf{k}'} F_{\mathbf{k},\mathbf{k}'} \Lambda_{\pm}(\mathbf{k}') \\ \times \left[\frac{1}{2} - n_F(\sqrt{\varepsilon_{\mathbf{k}',\pm}^2 + \Delta^2}) \right]. \quad (31)$$

From Eq. (30), one obtains that the triplet order parameter $\Delta_t(\mathbf{k})$ depends on the phase factor $e^{i\phi_{\mathbf{k}}}$ and hence the direction of the momentum, which is odd in the momentum. Thus, $\Delta_t(\mathbf{k})$ is the triplet p -wave order parameter. Specifically, this p -wave order parameter is in the $(p_x \pm ip_y)$ type.^{14,31,32,70} It is noted that if $F_{\mathbf{k},\mathbf{k}'}$ is arbitrarily taken to be momentum-independent, the triplet order parameter [Eq. (30)] is exactly zero due to the angle integration.

1. Momentum dependence of triplet p -wave order parameter

In this part, we analyze the momentum dependence of the triplet order parameter including the angular and magnitude dependencies, which is summarized in Fig. 5. In Fig. 5, when $n_e = 10n_0$, the \mathbf{d} -vectors of the triplet order parameter are plotted, defined as^{3,31,33}

$$\Delta_t(\mathbf{k}) = [\mathbf{d}(\mathbf{k}) \cdot \boldsymbol{\sigma}] i\sigma_y, \quad (32)$$

are plotted, with $\mathbf{d}(\mathbf{k}) = (d_x(\mathbf{k}), d_y(\mathbf{k}), d_z(\mathbf{k}))$. It is shown that only the in-plane components of the \mathbf{d} -vector are induced in (100) QWs. Specifically, in Figs. 5(a) and (b), it is shown that the $\hat{\mathbf{x}}$ and $\hat{\mathbf{y}}$ components of the induced triplet order parameter satisfies $d_x(\mathbf{k}) \propto -\cos \phi_{\mathbf{k}}$ and $d_y(\mathbf{k}) \propto \sin \phi_{\mathbf{k}}$, which is parallel to the effective magnetic field due to the SOC [Eq. (3)]. Thus, the induced triplet order parameter is stable due to the SOC.³² Moreover, the calculated results in Fig. 5 show that the induced triplet order parameter also depends on the magnitude of momentum or electron energy, which are further discussed in the following.

In Fig. 6, the energy dependence of the absolute value of the induced triplet order parameters $|\Delta_t(\mathbf{k})|$ is plotted when $n_e = 10n_0$ and $30n_0$, respectively. It is shown that with the increase of the electron energy, $|\Delta_t(\mathbf{k})|$ first increases from zero at $\mathbf{k} = 0$ and then decreases with a peak arising at moderate energy. This can be understood as follows. When $\mathbf{k} = 0$, from Eq. (30), $\Delta_t(\mathbf{k})$ equals to zero due to the angular integration over $\phi_{\mathbf{k}'}$. To further analyze the energy dependence of $|\Delta_t(\mathbf{k})|$, Eq. (30) can be simplified, which is similar to the situation of the Coulomb-interaction-induced singlet order parameter. It can be seen that $n_F(\sqrt{\varepsilon_{\mathbf{k}',\pm}^2 + \Delta^2})$ can be neglected in Eq. (30) when $\Delta \gg k_B T$. Furthermore, when $n_e \lesssim 20n_0$, the system lies in the singlet-band regime, and the magnitude of the triplet order parameter is written as

$$|\Delta_t(\mathbf{k})| \approx \frac{m^*}{16\pi^2} \int d\varepsilon_{\mathbf{k}'} d\phi_{\mathbf{k}'} F_{\mathbf{k},\mathbf{k}'} \cos(\phi_{\mathbf{k}'}) \Lambda_-(\mathbf{k}'). \quad (33)$$

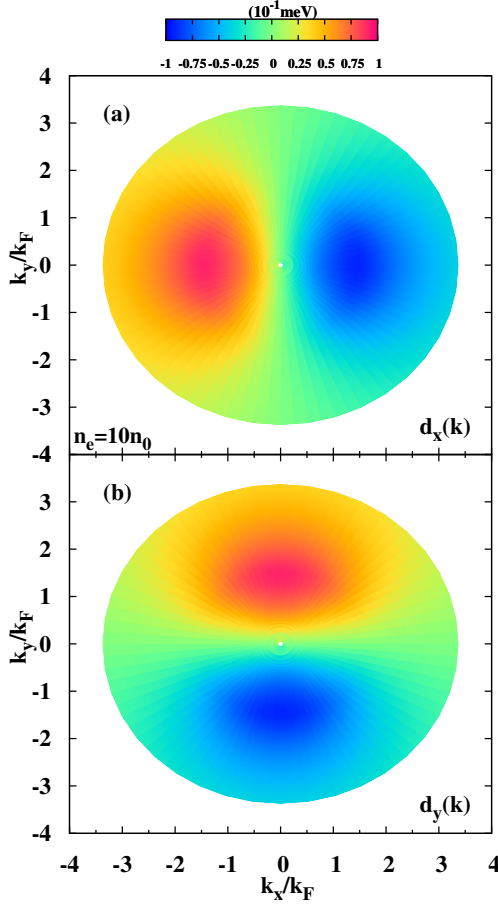


FIG. 5: (Color online) Momentum dependence of the \mathbf{d} -vectors. The electron density is $n_e = 10n_0$ with $k_F = 7.9 \times 10^7 \text{ m}^{-1}$. In (a) and (b), it is shown that the $\hat{\mathbf{x}}$ and $\hat{\mathbf{y}}$ components of the induced triplet order parameter satisfy $d_x(\mathbf{k}) \propto -\cos \phi_{\mathbf{k}}$ and $d_y(\mathbf{k}) \propto \sin \phi_{\mathbf{k}}$, respectively. Moreover, the calculated results show that the induced triplet order parameter also depends on the magnitude of momentum.

Whereas when $n_e \gtrsim 20n_0$, the system lies in the double-band regime, with the corresponding magnitude of the triplet order parameter written as

$$|\Delta_t(\mathbf{k})| \approx \frac{m^*}{16\pi^2} \int d\varepsilon_{\mathbf{k}'} d\phi_{\mathbf{k}'} F_{\mathbf{k},\mathbf{k}'} \cos(\phi_{\mathbf{k}'}) \times [\Lambda_-(\mathbf{k}') - \Lambda_+(\mathbf{k}')]. \quad (34)$$

Based on Eqs. (33) and (34), the energy dependencies of $|\Delta_t(\mathbf{k})|$ can be understood as follows.

We first address that when \mathbf{k} is very large, the Coulomb potential is efficiently suppressed, and hence the induced triplet order parameter tends to be zero when the energy tends to infinite. Accordingly, when $|\mathbf{k}| = 0$ and $|\mathbf{k}| \rightarrow \infty$, $|\Delta_t(\mathbf{k})| \rightarrow 0$. Therefore, there must exist non-monotonic behavior between $|\mathbf{k}| = 0$ and $|\mathbf{k}| \rightarrow \infty$, which is shown to be a peak at the moderate energy. Specifically, when $n = 10n_0$, the system lies in the single-band regime and the behavior of $|\Delta_t(\mathbf{k})|$ can be described by

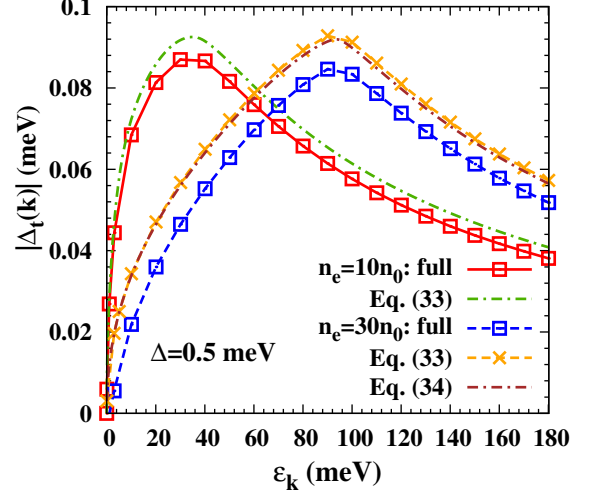


FIG. 6: (Color online) Energy dependence of the absolute value of the induced triplet order parameter $|\Delta_t(\mathbf{k})|$ when $n_e = 10n_0$ (the red solid curve with squares) and $30n_0$ (the blue dashed curve with squares). Furthermore, the green chain curve (yellow dashed curve with crosses) represents the calculated results based on Eq. (33) when $n_e = 10n_0$ ($n_e = 30n_0$). Moreover, from Eq. (34), the calculated result for $n_e = 30n_0$ is plotted by the purple chain curve.

Eq. (33) well. This is justified in Fig. 6 by the fact that the green chain curve calculated from Eq. (33) almost coincides with the full calculation represented by the red solid curve with squares. From Eq. (33), on one hand, one observes that when $|\mathbf{k}'| \approx |\mathbf{k}|$, the Coulomb potential is relatively strong. Accordingly, electrons with momentum $|\mathbf{k}'| \approx |\mathbf{k}|$ can play an important role in the induction of the triplet order parameter. On the other hand, when $\varepsilon_{\mathbf{k},-} = 0$, $\Lambda_-(\mathbf{k})$ is largest, which means the electron around the chemical potential can also play an important role in the induction of the triplet order parameter. When the two parts of the electrons, i.e., the electrons with momentum $|\mathbf{k}|$ and the ones around the chemical potential, are not the same, the induced triplet order parameter is expected to be small. However, with the increase of the momentum \mathbf{k} , there exists a “intersection” point that the two parts of the electrons are the same, where the peak arises in the energy dependence of $|\Delta_t(\mathbf{k})|$. Accordingly, from this simple picture, the position of the peak of $|\Delta_t(\mathbf{k})|$ in the energy dependence can be determined.

Specifically, one expects that in the single-band regime, the “intersection” point arises when the condition $k_c^2/(2m^*) - \alpha k_c - \mu \approx 0$ is satisfied, where k_c is the magnitude of the momentum at the “intersection” point. Therefore, the “intersection” point is estimated to be

$$\varepsilon_k^c \equiv k_c^2/(2m^*) \approx m^* \alpha^2 + \mu + \alpha \sqrt{2m^*(m^* \alpha^2/2 + \mu)}, \quad (35)$$

which labels the position of the peak. Here, we compare Eq. (35) with the full numerical calculations. From Eq. (35), when $n_e = 5n_0$, $10n_0$ and $20n_0$, the calculated peak position are at 27.0, 37.4 and 64.1 meV, respectively. They are very close to the corresponding ones from the full numerical calculations, which are 27.3, 35.1 and 63.4 meV. Furthermore, from Eq. (35), one obtains that when the electron density and hence the chemical potential increases, the position of the peak arises at higher energy.

When $n_e = 30n_0$, one expects that the system enters into the double-band regime. However, it is shown in Fig. 6 that the results calculated from Eqs. (34) and (33) almost coincide, denoted by the purple chain curve and yellow dashed curve with crosses, respectively. This indicates that the contribution from $E_{\mathbf{k},+}$ -band is negligible even when its population becomes significant. This is because even in the double-band regime, the average momentum of the populated electrons in $E_{\mathbf{k},+}$ -band is close to zero, which is much smaller than the ones in $E_{\mathbf{k},-}$ -band. This can be explicitly seen from Fig. 4 that the momentum corresponding to the intersection point between μ_3 and $E_{\mathbf{k},+}$ -band is close to zero. Specifically, the average momentum in $E_{\mathbf{k},+}$ -band is much smaller than the wave-vector due to the effective polarization function. Hence, the Coulomb potential experienced by the electron in $E_{\mathbf{k},+}$ -band can be treated as momentum-independent potential approximately, which does not contribute to the induction of the triplet order parameter due to the angle integration in Eq. (30).²⁵ In this situation, the system still lies in the single-band regime. Hence, the position of the peak is determined from Eq. (35), which is calculated to be 94.2 meV, again very close to the one from the full calculation, i.e., 93.7 meV.

2. Electron density dependence of triplet order parameter

In this part, we study the electron density dependence of the maximum value of the triplet order parameter Δ_t^m , shown in Fig. 7. It is seen that with the increase of the electron density, Δ_t^m first decreases at the low electron density $n_e \lesssim 3n_0$, then increases *slowly* at the moderate electron density $3n_0 \lesssim n_e \lesssim 20n_0$ and finally, decreases slowly when $n_e \gtrsim 20n_0$. Accordingly, a valley and an *extremely* weak peak appears at low and moderate electron densities, respectively. Nevertheless, when the Coulomb potential is taken to be independent on electron density in Eq. (30), it is shown in Fig. 7 by the green chain curve with circles (labeled by $\Delta_{t,C}^m$) that with the increase of the electron density, $\Delta_{t,C}^m$ first increases when $n_e \lesssim 3n_0$, then decreases rapidly when $3n_0 \lesssim n_e \lesssim 20n_0$, and finally decreases slowly when $n_e \gtrsim 20n_0$. One notices that all these features are very similar to the electron density dependence of the renormalized singlet order parameter, addressed in detail in Sec. IV A 2. The only difference is that when $n_e \gtrsim 20n_0$, the system actually lies in the

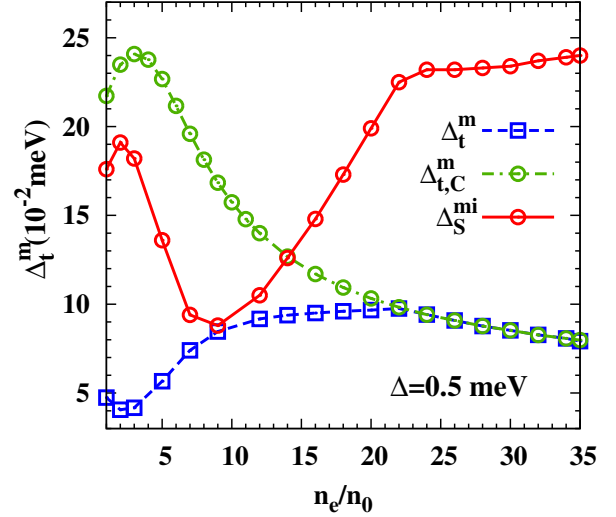


FIG. 7: (Color online) Electron density dependence of the maximum value of the induced triplet order parameter Δ_t^m , shown by the blue dashed curve with squares. The green chain curve with circles denoted by $\Delta_{t,C}^m$ represents the calculated results when the polarization function is taken to the one when $n_e = 35n_0$ in Eq. (30). Finally, the red solid curve with circles represents the minimum value of the renormalized singlet order parameter Δ_S^{mi} .

single-band regime with the electrons in $E_{\mathbf{k},+}$ -band being efficiently screened (refer to Sec. IV B 1). Above features can be understood as follows.

When the electron density is relatively low ($n_e \lesssim 3n_0$), with the increase of the electron density, the chemical potential increases slowly, but the strength of the Coulomb potential varies rapidly, with a valley appearing at the crossover between the non-degenerate and degenerate regimes. When the electron density is relatively high ($n_e \gtrsim 20n_0$), the effective polarization function becomes insensitive to the variation of the electron density, and hence with the increase of the electron density, the increase of the chemical potential influences the triplet pairing and causes the decrease of Δ_t^m . Finally, in the moderate regime ($3n_0 \lesssim n_e \lesssim 20n_0$), there exists competition between the Coulomb potential and triplet pairing, leading to a shallow peak.

Finally, we compare the magnitude of the renormalized singlet and induced triplet order parameters. In Fig. 7, the minimum and maximum values of the renormalized singlet ($\Delta_S^{mi} = \Delta - \Delta_s^m$) and triplet (Δ_t^m) order parameters are plotted by the red solid curve with circles and blue dashed curve with squares, respectively. Specifically, one observes that when the electron density $n_e \approx 8n_0$, Δ_S^{mi} and Δ_t^m become comparable. This provides an ideal condition to observe and distinguish these two order parameters in experiment. Moreover, with the magnitude comparable to the singlet one, the triplet order parameter can provide significant protection to the ground state and is promising to cause rich physics especially for the

elementary excitation.

V. SUMMARY AND DISCUSSION

In summary, we here demonstrated that the triplet p -wave superconductivity can be realized in the strong spin-orbit-coupled QWs in proximity to s -wave superconductor. It is analytically shown that the triplet order parameter is induced due to the e-e Coulomb and e-p interactions. Specifically, with the singlet order parameter from the superconducting proximity effect, not only can the singlet pairings exist from the proximity-induced order parameter, but also the triplet pairings are induced due to the SOC.²⁵ Then with the effective e-e interactions, the singlet order parameter is renormalized from the singlet pairings and the triplet order parameter is induced from the triplet pairings. All these can be systematically obtained from the derived effective BdG equation, in which the self-energies due to the e-e Coulomb and e-p interactions are proved to play the role of the singlet and triplet order parameters. Moreover, for the renormalized singlet order parameter, we reveal that it is suppressed because the singlet order parameter induced from the repulsive effective e-e interaction is always in opposite sign against the proximity-induced one. For the induced triplet order parameter, it is proved that it is odd in the momentum and is the p -wave one ($p_x \pm ip_y$).

We then perform the numerical calculations for the renormalized singlet and induced triplet order parameters in a specific material, i.e., strong spin-orbit-coupled InSb (100) QWs.^{61,62} In InSb QWs, the calculations show that at low temperature, the self-energy contributed by the e-p interaction is two orders of magnitude smaller than the one due to the e-e Coulomb interaction, and hence is negligible. Specifically, for the Coulomb-interaction-induced singlet order parameter, it only depends on the magnitude of the momentum, which decreases with the increase of the energy due to the suppression of the Coulomb interaction. For the induced triplet order parameter, it depends not only on the magnitude, but also on the angle of the momentum. Specifically, in the module dependence of the momentum, a peak shows up at the position determined by

$$k_c = m^* \alpha + \sqrt{2m^* \mu + m^2 \alpha^2} \quad (36)$$

where the electron energy just corresponds to the chemical potential. In the angular dependence of momentum, it is revealed that the \mathbf{d} -vector of the induced triplet order parameter is parallel to the effective magnetic field due to the SOC, and hence is protected by the SOC.³² Finally, it is found that with proper electron density ($n_e \approx 8 \times 10^{14} \text{ cm}^{-2}$), the maximum of the induced triplet order parameter and the minimum of the renormalized singlet order parameter are comparable. This provides an ideal condition to observe and distinguish these order parameters experimentally.

Finally, we discuss the possibilities to realize the triplet pairing and triplet order parameter in other systems including the symmetric (110) and (111) QWs. For the (110) symmetric QWs, the Dresselhaus SOC only has the out-of-plane component, which is expressed as $H_{\text{soc}}^{(110)} = h_z(\mathbf{k})\sigma_z$ with $h_z(\mathbf{k})$ being the effective magnetic field.⁷¹⁻⁷⁷ In this situation, the triplet pairing and triplet order parameter are exactly zero. For the (111) symmetric QWs, the Dresselhaus SOC is expressed as $H_{\text{soc}}^{(111)} = \mathbf{h}(\mathbf{k}) \cdot \boldsymbol{\sigma}$ with $\mathbf{h}(\mathbf{k}) = (h_x(\mathbf{k}), h_y(\mathbf{k}), h_z(\mathbf{k}))$.^{78,79} The \mathbf{d} -vector of the triplet order parameter is parallel to the in-plane components of the SOC, whose strength is influenced by the out-of-plane component of the SOC because of its influence on the energy spectra.

Acknowledgments

This work was supported by the National Natural Science Foundation of China under Grant No. 11334014 and 6141136001, the National Basic Research Program of China under Grant No. 2012CB922002 and the Strategic Priority Research Program of the Chinese Academy of Sciences under Grant No. XDB01000000.

Appendix A: SINGLE-PARTICLE TUNNELING INDUCED SELF-ENERGY

The single-particle tunneling Hamiltonian between the QWs and s -wave superconductor is given as

$$\hat{H}_T = \int d\mathbf{r} \hat{\Psi}^\dagger(\mathbf{r}) \hat{T} \hat{\tau}_3 \hat{\Phi}(\mathbf{r}), \quad (\text{A1})$$

where $\hat{T} = t$ with t being the element of the tunneling matrix, taken to be real in this work. One notes that Eq. (A1) is widely used in the study of the quantum nanowire in proximity to superconductor in the study of Majorana zero mode.⁵⁵⁻⁵⁷

Following the derivation in Refs. 55,56,67, the self-energy in the Matsubara representation due to the single-particle tunneling effect is calculated based on Hamiltonian Eq. (A1) and is given by

$$\Sigma_s(\tau_1 - \tau_2, \mathbf{r}_1 - \mathbf{r}_2) = \hat{T} G_S(\tau_1 - \tau_2, \mathbf{r}_1 - \mathbf{r}_2) \hat{T}^\dagger. \quad (\text{A2})$$

In Eq. (A2), \mathbf{r}_1 and \mathbf{r}_2 are 2D in QWs, which corresponds to the interface between QWs and superconductors; $G_S(\tau_1 - \tau_2, \mathbf{r}_1 - \mathbf{r}_2)$ is the Green function in the s -wave superconductor, which is defined as

$$G_S(\tau_1 - \tau_2, \mathbf{r}_1 - \mathbf{r}_2) = -\hat{\tau}_3 \langle T_\tau \hat{\Phi}(\tau_1, \mathbf{r}_1) \hat{\Phi}^\dagger(\tau_2, \mathbf{r}_2) \rangle. \quad (\text{A3})$$

In the frequency-momentum space, the self-energy due to the single-particle tunneling effect is further written as^{55-57,67}

$$\Sigma_s(i\omega_m, \mathbf{k}) = \hat{T} G_S(i\omega_m, \mathbf{k}) \hat{T}^\dagger, \quad (\text{A4})$$

in which $G_S(i\omega_m, \mathbf{k}) = \int \frac{dp_z}{2\pi} G_S(i\omega_m, \mathbf{p})$ with $\mathbf{p} = (\mathbf{k}, p_z) = (k_x, k_y, p_z)$. Specifically, in s -wave superconductor,

$$G_S(i\omega_m, \mathbf{p}) = \frac{1}{(i\omega_m)^2 - \zeta_{\mathbf{p}}^2 - |\Delta_0|^2} \times \begin{pmatrix} i\omega_m + \zeta_{\mathbf{p}} & 0 & 0 & \Delta_0 \\ 0 & i\omega_m + \zeta_{\mathbf{p}} & -\Delta_0 & 0 \\ 0 & \Delta_0^* & -i\omega_m + \zeta_{\mathbf{p}} & 0 \\ -\Delta_0^* & 0 & 0 & -i\omega_m + \zeta_{\mathbf{p}} \end{pmatrix}, \quad (\text{A5})$$

where $\zeta_{\mathbf{p}} = \frac{\mathbf{p}^2}{2m} - \tilde{\mu}$. Accordingly, from Eqs. (A4) and (A5), one obtains the self-energy due to single-particle tunneling effect in frequency-momentum space

$$\Sigma_s(i\omega_m, \mathbf{k}) = t^2 \int \frac{dp_z}{2\pi} \frac{1}{(i\omega_m)^2 - \zeta_{\mathbf{p}}^2 - |\Delta_0|^2} \times \begin{pmatrix} i\omega_m + \zeta_{\mathbf{p}} & 0 & 0 & \Delta_0 \\ 0 & i\omega_m + \zeta_{\mathbf{p}} & -\Delta_0 & 0 \\ 0 & \Delta_0^* & -i\omega_m + \zeta_{\mathbf{p}} & 0 \\ -\Delta_0^* & 0 & 0 & -i\omega_m + \zeta_{\mathbf{p}} \end{pmatrix}. \quad (\text{A6})$$

From Eq. (A6), one observes that $\Sigma_s(i\omega_m, \mathbf{k})$ generally depends on the Matsubara frequency and momentum, and hence the real frequency after the analytical continuation $i\omega_m \rightarrow \omega + i0^+$. Specifically, from the effective BdG equation [Eq. (16)], in $\Sigma_s(\omega, \mathbf{k})\hat{\tau}_3$, the diagonal terms only modifies the effective mass of the electron and shifts zero-energy point of the system, which are neglected in our analysis; whereas the off-diagonal terms act as the effective *even-frequency* and *even-momentum* singlet order parameter.^{55–57,67} Accordingly, we obtain the tunneling-induced order parameter,

$$\Delta(i\omega_m, \mathbf{k}) = -t^2 \int \frac{dp_z}{2\pi} \frac{\Delta_0}{(i\omega_m)^2 - \zeta_{\mathbf{p}}^2 - |\Delta_0|^2}. \quad (\text{A7})$$

Appendix B: COULOMB SCREENING

In this appendix, we present the calculation of the Coulomb screening from the linear response theory,^{58–60} in which both the *strong* SOC and proximity-induced singlet order parameter are considered explicitly. In the Matsubara representation, the dielectric constant in the RPA approximation is calculated by

$$\varepsilon_{\text{RPA}}(\mathbf{k}, i\omega_n) = 1 - \tilde{V}_{\mathbf{k}} P^{(1)}(\mathbf{k}, i\omega_n), \quad (\text{B1})$$

with $\tilde{V}_{\mathbf{k}}$ being the unscreened Coulomb potential. In Eq. (B1),

$$P^{(1)}(\mathbf{k}, i\omega_n) = - \int_0^\beta d\tau e^{i\omega_n \tau} \langle T_\tau \hat{\rho}(\mathbf{k}, \tau) \hat{\rho}(-\mathbf{k}, 0) \rangle, \quad (\text{B2})$$

in which $\hat{\rho}(\mathbf{k})$ is the density operator. Eq. (B2) is further expressed by the 4×4 Green function [Eq. (19)] as

$$P^{(1)}(\mathbf{k}, i\omega_n) = \frac{1}{2\beta} \sum_{\mathbf{k}', n'} \text{Tr} \left[G(\mathbf{k} + \mathbf{k}', \omega_n + \omega_{n'}) G(\mathbf{k}', \omega_{n'}) \right]. \quad (\text{B3})$$

In our calculation, we focus on the long-wave and static situations, i.e., $\mathbf{k} \rightarrow 0$ and $\omega \rightarrow 0$ in Eq. (B3). To reveal the effects of the SOC and proximity-induced singlet order parameter, we also calculate the normal case by setting α and/or Δ to be zero in Eq. (B3). These results are summarized in Fig. 8 in the electron density dependencies of the effective polarization function, which is defined in Eq. (27).

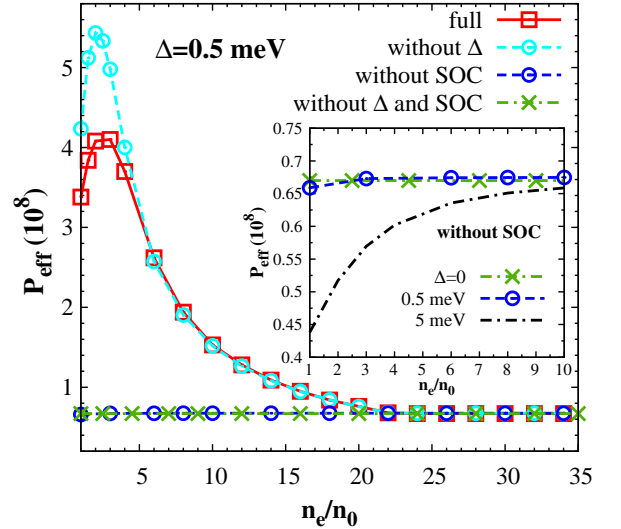


FIG. 8: (Color online) Density dependence of the effective polarization function P_{eff} . The red solid curve with squares represents the full calculation with the SOC and Δ explicitly included. Furthermore, the situations without Δ , without the SOC, and without Δ and the SOC are denoted by the cyan dashed curve with circles, the blue dashed curve with circles and the green chain curve with crosses, respectively. The inset zooms the electron density dependence of the effective polarization function when the SOC is set to be zero, with $\Delta = 0$ (the green chain curve with crosses), 0.5 meV (the blue dashed curve with circles) and 5 meV (the black chain curve), respectively.

In Fig. 8, when the SOC and Δ are explicitly included in the calculation, it is shown by the red solid curve with squares that there exists a peak in the electron density dependence of P_{eff} , which appears at the crossover between the non-degenerate and degenerate regimes. This is in contrast to the case without the SOC and Δ , referred to as the normal case. This is shown by the green chain curve with crosses that when α and Δ are set to be zero, P_{eff} becomes insensitive to the electron density. This insensitivity arises from the fact that when α and Δ are set to be zero, with the electron densities we study here, the system always lies in the degenerate regime;

whereas with the SOC included, the system actually lies in the non-degenerate regime when $n_e \lesssim 3n_0$, as shown in the inset of Fig. 3.

To clearly reveal the effects of the SOC and Δ in the Coulomb screening, we further calculate the cases with only the SOC or Δ included in Eq. (B3). In Fig. 8, it is shown by the cyan dashed curve with circles that when Δ is set to be zero (hence only the SOC is included), the effective polarization function also shows a peak in the electron density dependence. Specifically, the peak is significantly enhanced at the crossover between the non-degenerate and degenerate regimes compared to the full calculation represented by the red solid curve with squares. This indicates that Δ can suppress the screening effect. Nevertheless, when the SOC is set to be

zero with $\Delta = 0.5$ meV, it is shown by the blue dashed curve with circles that P_{eff} becomes very close to the normal case denoted by the green chain curve with crosses. Therefore, it is the joint effects of the SOC and singlet order parameter that cause the efficient suppression of the Coulomb screening here. Actually, the singlet order parameter alone can also suppress the Coulomb screening. Nevertheless, it is not obvious in the weak coupling limit when Δ is much smaller than the Fermi energy, but significant when Δ is large. In the inset of Fig. 8, we show that when $\alpha = 0$, compared to the case with $\Delta = 0$, the screening with $\Delta = 5$ meV represented by the black chain curve shows that P_{eff} is significantly suppressed at low electron density.

-
- * Author to whom correspondence should be addressed; Electronic address: mwwwu@ustc.edu.cn.
- ¹ R. Meservey and P. M. Tedrow, Phys. Rep. **238**, 173 (1994).
 - ² A. I. Buzdin, Rev. Mod. Phys. **77**, 935 (2005).
 - ³ F. S. Bergeret, A. F. Volkov, and K. B. Efetov, Rev. Mod. Phys. **77**, 1321 (2005).
 - ⁴ A. Buzdin, Rev. Mod. Phys. **77**, 935 (2005).
 - ⁵ M. Eschrig, Phys. Today **64**, 43 (2011).
 - ⁶ J. Linder and J. W. A. Robinson, Nat. Phys. **11**, 307 (2015).
 - ⁷ *Semiconductor Spintronics and Quantum Computation*, edited by D. D. Awschalom, D. Loss, and N. Samarth (Springer, Berlin, 2002).
 - ⁸ I. Žutić, J. Fabian, and S. D. Sarma, Rev. Mod. Phys. **76**, 323 (2004).
 - ⁹ J. Fabian, A. Matos-Abiad, C. Ertler, P. Stano, and I. Žutić, Acta Phys. Slov. **57**, 565 (2007).
 - ¹⁰ M. W. Wu, J. H. Jiang, and M. Q. Weng, Phys. Rep. **493**, 61 (2010).
 - ¹¹ *Handbook of Spin Transport and Magnetism*, edited by E. Y. Tsymbal and I. Žutić (Boca Raton, FL: CRC press, 2011).
 - ¹² A. P. Mackenzie, R. K. W. Haselwimmer, A. W. Tyler, G. G. Lonzarich, Y. Mori, S. Nishizaki, and Y. Maeno, Phys. Rev. Lett. **80**, 161 (1998).
 - ¹³ K. Ishida, Y. Kitaoka, K. Asayama, S. Ikeda, S. Nishizaki, Y. Maeno, K. Yoshida, and T. Fujita, Phys. Rev. B **56**, R505 (1997).
 - ¹⁴ T. M. Rice and M. Sigrist, J. Phys., Condens. Matter **7**, L643 (1995).
 - ¹⁵ I. Eremin, D. Manske, S. G. Ovchinnikov, and J. F. Annett, Ann. Phys. **13**, 149 (2004).
 - ¹⁶ Y. Maeno, H. Hashimoto, K. Yoshida, S. Nishizaki, T. Fujita, J. G. Bednorz, and F. Lichtenberg, Nature (London) **372**, 532 (1994).
 - ¹⁷ N. Read and D. Green, Phys. Rev. B **61**, 10267 (2000).
 - ¹⁸ D. A. Ivanov, Phys. Rev. Lett. **86**, 268 (2001).
 - ¹⁹ A. P. Mackenzie and Y. Maeno, Rev. Mod. Phys. **75**, 657 (2003).
 - ²⁰ V. M. Edelstein, Phys. Rev. B **67**, 020505 (2001).
 - ²¹ M. Alidoust and J. Linder, Phys. Rev. B **82**, 224504 (2010).
 - ²² F. S. Bergeret and I. V. Tokatly, Phys. Rev. Lett. **110**, 117003 (2013); Phys. Rev. B **89**, 134517 (2014).
 - ²³ A. D. Bernardo, S. Diesch, Y. Gu, J. Linder, G. Divitini, C. Ducati, E. Scheer, M. G. Blamire, and J. W. A. Robinson, Nat. Commun. **6**, 8053 (2015).
 - ²⁴ Y. Kalcheim, O. Millo, A. D. Bernardo, A. Pal, and J. W. A. Robinson, Phys. Rev. B **92**, 060501(R) (2015).
 - ²⁵ Gor'kov and Rashba, Phys. Rev. Lett. **87**, 037004 (2001).
 - ²⁶ Z. H. Yang, J. Wang, and K. S. Chan, Supercond. Sci. Technol. **22**, 055012 (2009).
 - ²⁷ X. Liu, J. K. Jain, and C. X. Liu, Phys. Rev. Lett. **113**, 227002 (2014).
 - ²⁸ C. R. Reeg and D. L. Maslov, Phys. Rev. B **92**, 134512 (2015).
 - ²⁹ S. Jacobsen, I. Kulagina, and J. Linder, arXiv:1510.02488.
 - ³⁰ C. Triola, D. M. Badiane, A. V. Balatsky, and E. Rossi, arXiv:1512.03068.
 - ³¹ M. Sigrist and K. Ueda, Rev. Mod. Phys. **63**, 239 (1991).
 - ³² P. A. Frigeri, D. F. Agterberg, A. Koga, and M. Sigrist, Phys. Rev. Lett. **92**, 097001 (2004).
 - ³³ E. Bauer and M. Sigrist, *Non-centrosymmetric superconductors: introduction and overview*, (Springer Science and business Media, 2012).
 - ³⁴ A. Layzer and D. Fay, Int. J. Magn. **1**, 135 (1971).
 - ³⁵ P. W. Anderson and W. F. Brinkman, Phys. Rev. Lett. **30**, 1108 (1973).
 - ³⁶ W. F. Brinkman, J. W. Serene, and P. W. Anderson, Phys. Rev. A **10**, 2386 (1974).
 - ³⁷ V. L. Berezinskii, JETP Lett **20**, 287 (1974).
 - ³⁸ Y. A. Bychkov and E. I. Rashba, J. Phys. C **17**, 6039 (1984).
 - ³⁹ Y. A. Bychkov, JETP Lett. **39**, 78 (1984).
 - ⁴⁰ G. Dresselhaus, Phys. Rev. **100**, 580 (1955).
 - ⁴¹ L. N. Bulaevskii, V. V. Kuzii, and A. A. Sobyenin, Pis'ma Zh. Eksp. Teor. Fiz. **25**, 314 (1977) [JETP Lett. **25**, 290 (1977)].
 - ⁴² A. I. Buzdin, L. N. Bulaevskii, and S. V. Panyukov, Pis'ma Zh. Eksp. Teor. Fiz. **35**, 147 (1982) [JETP Lett. **35**, 178 (1982)].
 - ⁴³ V. V. Ryazanov, V. A. Oboznov, A. Y. Rusanov, A. V. Veretennikov, A. A. Golubov, and J. Aarts, Phys. Rev. Lett. **86**, 2427 (2001).
 - ⁴⁴ M. Alidoust, J. Linder, G. Rashedi, T. Yokoyama, and A. Sudbø, Phys. Rev. B **81**, 014512 (2010).

- ⁴⁵ P. G. De Gennes, *Rev. Mod. Phys.* **36**, 225 (1964).
- ⁴⁶ H. Takayanagi and T. Kawakami, *Phys. Rev. Lett.* **54**, 2449 (1985).
- ⁴⁷ T. Akazaki, H. Takayanagi, J. Nitta, and T. Enoki, *Appl. Phys. Lett.* **68**, 418 (1996).
- ⁴⁸ K. M. H. Lenssen, M. Matters, and C. J. P. M. Harmans, *Appl. Phys. Lett.* **63**, 2079 (1993).
- ⁴⁹ T. D. Moore and D. A. Williams, *Phys. Rev. B* **59**, 7308 (1999).
- ⁵⁰ Z. Wan, A. Kazakov, M. J. Manfra, L. N. Pfeiffer, K. W. West, and L. P. Rokhinson, *Nat. Commun.* **6**, 7426 (2015).
- ⁵¹ D. A. Ivanov, *Phys. Rev. Lett.* **86**, 268 (2001).
- ⁵² A. Stern, F. von Oppen, and E. Mariani, *Phys. Rev. B* **70**, 205338 (2004).
- ⁵³ J. Alicea, Y. Oreg, G. Refael, F. Von Oppen, and M. Fisher, *Nat. Phys.* **7**, 412 (2011).
- ⁵⁴ C. Beenakker, *Annu. Rev. Condens. Matter Phys.* **4**, 113 (2013).
- ⁵⁵ J. D. Sau, R. M. Lutchyn, S. Tewari, and S. Das Sarma, *Phys. Rev. B* **84**, 144522 (2011).
- ⁵⁶ T. D. Stanescu, R. M. Lutchyn, and S. Das Sarma, *Phys. Rev. B* **84**, 144522 (2011).
- ⁵⁷ H. Y. Hui, P. M. R. Brydon, J. D. Sau, S. Tewari, and S. Das Sarma, *Sci. Rep.* **5**, 8880 (2015).
- ⁵⁸ A. L. Fetter and J. D. Walecka, *Quantum Theory of Many Particle Systems* (McGraw-Hill, New York, 1971).
- ⁵⁹ G. D. Mahan, *Many Particle Physics* (Plenum, New York, 1990).
- ⁶⁰ A. A. Abrikosov, L. P. Gorkov, and I. E. Dzyaloshinski, *Methods of Quantum Field Theory in Statistical Physics* (Prentice Hall, Englewood Cliffs, N. J., 1963).
- ⁶¹ *Semiconductors*, Landolt-Börnstein, New Series, Vol. 17a, ed. by O. Madelung (Springer, Berlin, 1987).
- ⁶² J. M. Jancu, R. Scholz, E. A. de Andrada e Silva, and G. C. L. Rocca, *Phys. Rev. B* **72**, 193201 (2005).
- ⁶³ J. Zhou, J. L. Cheng, and M. W. Wu, *Phys. Rev. B* **75**, 045305 (2007).
- ⁶⁴ L. Jiang and M. W. Wu, *Phys. Rev. B* **72**, 033311 (2005).
- ⁶⁵ R. E. Prange, *Phys. Rev.* **129**, 2495 (1963).
- ⁶⁶ P. Vogl, in *Physics of Nonlinear Transport in Semiconductor*, edited by K. Ferry, J. R. Barker, and C. Jacoboni (Plenum, New York, 1980).
- ⁶⁷ J. Danon and K. Flensberg, *Phys. Rev. B* **91**, 165425 (2015).
- ⁶⁸ By considering the e-e Coulomb interaction for the electrons between the QWs and *s*-wave superconductor, the singlet pairings in *s*-wave superconductor can also induce the singlet order parameter in QWs by providing the self-energy [Eq. (16)].
- ⁶⁹ A. Haim, A. Keselman, E. Berg, and Y. Oreg, *Phys. Rev. B* **89**, 220504(R) (2014).
- ⁷⁰ A. J. Leggett, *Rev. Mod. Phys.* **47**, 331 (1975).
- ⁷¹ Y. Ohno, R. Terauchi, T. Adachi, F. Matsukura, and H. Ohno, *Phys. Rev. Lett.* **83**, 4196 (1999); *Physica E* **6**, 817 (2000); T. Adachi, Y. Ohno, F. Matsukura, and H. Ohno, *Physica E* **10**, 36 (2001).
- ⁷² M. W. Wu and M. Kuwata-Gonokami, *Solid State Commun.* **121**, 509 (2002).
- ⁷³ S. Döhrmann, D. Hägele, J. Rudolph, M. Bichler, D. Schuh, and M. Oestreich, *Phys. Rev. Lett.* **93**, 147405 (2004).
- ⁷⁴ G. M. Müller, M. Römer, D. Schuh, W. Wegscheider, J. Hübner, and M. Oestreich, *Phys. Rev. Lett.* **101**, 206601 (2008).
- ⁷⁵ I. V. Tokatly and E. Y. Sherman, *Phys. Rev. B* **82**, 161305(R) (2010).
- ⁷⁶ Y. Zhou, T. Yu, and M. W. Wu, *Phys. Rev. B* **87**, 245304 (2013).
- ⁷⁷ T. Yu and M. W. Wu, *Phys. Rev. B* **89**, 045303 (2014).
- ⁷⁸ R. Winkler, *Phys. Rev. B* **69**, 045317 (2004).
- ⁷⁹ B. Y. Sun, P. Zhang, and M. W. Wu, *J. Appl. Phys.* **108**, 093709 (2010).